journal of the mechanical behavior of biomedical materials 141 (2023) 105752

Contents lists available at ScienceDirect

Journal of the Mechanical Behavior of Biomedical Materials

journal homepage: www.elsevier.com/locate/jmbbm

Tri-layered constitutive modelling unveils functional differences between the pig ascending and lower thoracic aorta

A. Giudici [a,b], B. Spronck [b,c], I.B. Wilkinson [d], A.W. Khir [a,e,*]

[a] Brunel Institute for Bioengineering, Brunel University London, Kingston Lane, Uxbridge, UB8 3PH, United Kingdom
[b] Department of Biomedical Engineering, CARIM School for Cardiovascular Diseases, Maastricht University, Universiteitssingel 40, Maastricht, 6229 ER, the Netherlands
[c] Macquarie Medical School, Faculty of Medicine, Health and Human Sciences, Macquarie University, Macquarie Park, Sydney, NSW, 2109, Australia
[d] Division of Experimental Medicine and Immunotherapeutics, University of Cambridge, Hills Road, Cambridge, CB2 0QO, United Kingdom
[e] Department of Engineering, Durham University, Durham, DH1 3LE, United Kingdom

ARTICLE INFO

Keywords:
Tri-layered arterial wall modelling
Layer-specific arterial mechanics
Thoracic aorta
Ascending aorta
Constitutive modelling

ABSTRACT

The arterial wall's tri-layered macroscopic and layer-specific microscopic structure determine its mechanical properties, which vary at different arterial locations. Combining layer-specific mechanical data and tri-layered modelling, this study aimed to characterise functional differences between the pig ascending (AA) and lower thoracic aorta (LTA).

AA and LTA segments were obtained for n=9 pigs. For each location, circumferentially and axially oriented intact wall and isolated layer strips were tested uniaxially and the layer-specific mechanical response modelled using a hyperelastic strain energy function. Then, layer-specific constitutive relations and intact wall mechanical data were combined to develop a tri-layered model of an AA and LTA cylindrical vessel, accounting for the layer-specific residual stresses. AA and LTA behaviours were then characterised for *in vivo* pressure ranges while stretched axially to *in vivo* length.

The media dominated the AA response, bearing>2/3 of the circumferential load both at physiological (100 mmHg) and hypertensive pressures (160 mmHg). The LTA media bore most of the circumferential load at physiological pressure only (57±7% at 100 mmHg), while adventitia and media load bearings were comparable at 160 mmHg. Furthermore, increased axial elongation affected the media/adventitia load-bearing only at the LTA.

The pig AA and LTA presented strong functional differences, likely reflecting their different roles in the circulation. The media-dominated compliant and anisotropic AA stores large amounts of elastic energy in response to both circumferential and axial deformations, which maximises diastolic recoiling function. This function is reduced at the LTA, where the adventitia shields the artery against supra-physiological circumferential and axial loads.

1. Introduction

The mechanical properties of the arterial wall vary considerably along the aorta. It is generally accepted that the wall material stiffness increases distally (R. Cox, 1978; Haskett et al., 2010; Learoyd and Taylor, 1966; Peña et al., 2017). These changes are likely to reflect differences at macro- and micro-structural levels that are in turn related to the specific haemodynamic function a segment of the aorta plays and possibly arise as a consequence of different blood flow patterns in the developmental phase of the arterial tree (Dinardo et al., 2014; Lu et al., 2001). At a macroscopic level, the arterial wall is organised in three concentric layers (intima, media and adventitia) that play different roles in arterial function. While the intima *per se* offers negligible contribution to intact wall mechanical load bearing of healthy arteries (Butcher, 1960; Giudici et al., 2021a), its endothelial cells sense the blood flow-induced shear stress, triggering signalling pathways that ultimately result in vaso-constriction/dilation (Krüger-Genge et al., 2019). The media is responsible for the compliant behaviour (i.e., the mechanical response to loads) of arteries at mean physiological pressures, dampening the strong oscillation of blood pressure that results from the intermittent cardiac pumping action (Wolinsky and Glagov, 1964). On the other hand, the adventitia works as a protective sleeve that prevents

* Corresponding author. Department of Engineering, Durham University, Lower Mountjoy, South Road, Durham, DH1 3LE, UK.
E-mail address: ashraf.w.khir@durham.ac.uk (A.W. Khir).

https://doi.org/10.1016/j.jmbbm.2023.105752
Received 18 November 2022; Received in revised form 22 February 2023; Accepted 1 March 2023
Available online 2 March 2023

rupture at supraphysiological pressure (Burton, 1954; Krasny et al., 2017). The relative thickness of the three layers varies along the aorta and, more generally, the arterial tree (Peña et al., 2015; Sokolis, 2019), affecting the layer-specific contribution to the overall wall mechanical response.

At a microscopic level, each layer is characterised by a complex structure (Giudici et al., 2021b) where the arrangements and concentrations of the wall constituents, mainly collagen and elastin, determine its passive mechanical behaviour. Changes in these constituents along the aorta have long been known; e.g., the elastin volume fraction is preponderant over collagen only in the proximal thoracic aorta and decreases quite abruptly below the diaphragm (Apter et al., 1966; R. H. Cox, 1978; Fischer and Llaurado, 1966; Harkness et al., 1957). Further, *ex vivo* studies have shown that the knowledge of the relative amount of collagen and elastin is not sufficient to predict inter-regional differences in wall mechanics (R. H. Cox, 1978). This suggest that regional differences in the constituent's microstructural arrangements are equally important to relative content in defining the macroscopic behaviour of arteries.

The isolation and tensile testing of individual arterial layers is a useful technique that allows investigating how inter-regional differences in layers' microstructure affects their mechanical properties. This experimental technique has been used at different locations of the arterial tree and in different species, including the human thoracic and abdominal aorta (Teng et al., 2015; Weisbecker et al., 2012), carotid artery (Sommer et al., 2010), coronaries (Holzapfel et al., 2005) and ascending aortic aneurysm (Deveja et al., 2018; Sassani et al., 2015), and the pig descending thoracic aorta (Giudici et al., 2021a; Giudici and Spronck, 2022; Peña et al., 2015). Further, fitting the experimental data using constitutive models whose parameters aim to describe the mechanical behaviour of the wall constituents (typically elastin and collagen) provides additional quantitative information on region- and layer-specific arterial structure-mechanics (Peña et al., 2015; Weisbecker et al., 2012).

While assessing the inter-regional differences in layer-specific mechanical properties can provide some insight into inter-regional differences in intact wall behaviour, residual stresses complicate the relationship between layer-specific and intact wall mechanics. The existence of residual stresses was first observed in circumferentially oriented wall strips (Chuong and Fung, 1986; Vaishnav and Vossoughi, 1983): when a single radial cut is performed on an arterial ring, this deforms into an arc shape. This configuration is typically defined *via* the opening angle (OA); traditionally defined as the angle that connects the end-points of the arc to the mid-length of the sample (Rachev and Greenwald, 2003). Later, experimental studies proved the existence of axial residual stresses; axially oriented arterial strips exhibit a curvature in the radial-axial plane when left to equilibrate in physiological saline solution (Holzapfel and Ogden, 2010). Therefore, all three arterial layers can be subjected to precompression or pretension in all three principal directions (i.e., circumferential, axial and radial) so that their mechanical responses when part of the wall might differ from the ones they exhibit when isolated.

We recently introduced an experimental/modelling framework that allows estimation of layer-specific residual deformations from layer-specific and intact wall uniaxial mechanical data (Giudici et al., 2021a). The definition of a tri-layered constitutive model of a cylindrical vessel allows simulating physiological loading conditions, thus providing the link between the layer-specific mechanical response and the macroscopic behaviour of the wall *in vivo*. Using the proposed methodology, this study aimed to investigate how inter-regional differences in layer-specific mechanics determine functional differences between aortic locations, specifically defined in this study, the ascending aorta (AA) and lower thoracic aorta (LTA).

2. Methods

2.1. Experimental protocol

2.1.1. Sample preparation

n=17 pig plucks (i.e., the content of the thorax) were purchased from a local abattoir (Samples for School, UK). Nine aortae were used for the uniaxial mechanical testing, while the remaining eight were used for opening angle (OA) experiments. The age of the animal at the time of excising the samples was between 6 and 12 months. The aortae were carefully isolated from the surrounding tissues using a scalpel and stored in a lab freezer at the temperature of −20 °C until the day of the testing. On the day of testing, aortae were left to thaw at room temperature (~20 °C) and at least two circumferentially oriented and two longitudinally oriented ~25 mm long and ~5 mm wide strips were cut from two aortic regions: 1) AA, and 2) LTA corresponding to the segment of aorta at the level of the intercostal arteries. Loose periadventitial connective tissue and fat were carefully removed using a scalpel to ensure a clear identification of the adventitial outer boundary. Then, the undeformed width and thickness of each strip were measured three times along the length of the sample using a digital micrometer (model 243–6846, RS Components Ltd., UK). The average of the three measurements was used for further analysis. The actual length of the strip was also measured with a digital calliper.

2.1.2. Determination of the opening angle

The wall and layer-specific OAs were measured on circumferentially oriented strips only. Arterial rings were placed in petri dishes filled with saline solution (NaCl 0.9%) kept at a temperature of 37 °C. Then, a single radial cut was performed to release the ring residual stresses. Cut-open rings were let to equilibrate for 30 min in saline solution at 37 °C (Holzapfel et al., 2002; Sokolis, 2019) and then photographs (Nikon 5600D equipped with a Sigma 18–200 mm zoom lens) of the samples (cross-sectional view) were taken from the top. Finally, OAs, defined as the angle formed by connecting the two endpoints of the cut-open sample to the midpoint along its length in the circumferential-radial plane, were measured using the images processing software ImageJ.

2.1.3. Mechanical testing

Each strip was then mounted on a uniaxial tensiometer (MFS Stage equipped with 20N load cell, Linkam Scientific Instruments Ltd., UK) equipped with serrated grips. To obtain a repeatable force-length relationship, samples were first subjected to a preconditioning protocol of five loading/unloading stretching sweeps between the unloaded state and a force corresponding to a Cauchy stress of approximately 250 kPa. After preconditioning, the distance between the jaws was finely adjusted until the sample laid horizontally (this step required the application of a force <0.020 N), then the strips were stretched at a speed of 100 μm/s until a Cauchy stress of 250 kPa (defined as force over deformed cross-sectional area, see Eq. (9)) was reached. Strips were then separated into the three anatomical layers using tweezers as described previously (Giudici et al., 2021a). For all samples, the layer separation protocol consisted in 1) peeling the adventitia from the intima-media and 2) carefully isolating the intima from the media. In case of the unsuccessful separation of one layer, this was replaced with one obtained from an adjacent strip of aortic tissue. The unloaded thickness and width of the isolated layers were measured three times along their length and the average was considered for further analysis. Furthermore, the length of the isolated layer strip was measured and used to experimentally quantify the layer-specific prestretch (Table 1). The testing protocol used for isolated layers was identical to that used on the intact wall.

2.2. Constitutive modelling

2.2.1. Tri-layered wall model

We recently introduced a constitutive modelling framework that

Table 1
Experimental and modelled layer pre-stretches.

Ascending aorta						
	Intima		Media		Adventitia	
	$\widehat{\lambda}^{i}_{\mathscr{X}}$	$\widehat{\lambda}^{i}_{\mathscr{Z}}$	$\widehat{\lambda}^{m}_{\mathscr{X}}$	$\widehat{\lambda}^{m}_{\mathscr{Z}}$	$\widehat{\lambda}^{a}_{\mathscr{X}}$	$\widehat{\lambda}^{a}_{\mathscr{Z}}$
Experimental	0.97 ± 0.01	1.00 ± 0.02	1.00 ± 0.01	1.05 ± 0.02	0.97 ± 0.01	0.98 ± 0.03
Modelled	0.96 ± 0.02	1.01 ± 0.05	1.03 ± 0.01	1.03 ± 0.01	1.00 ± 0.01	0.99 ± 0.02
	Λ^{i}_{Θ}	Λ^{i}_{Z}	Λ^{m}_{Θ}	Λ^{m}_{Z}	Λ^{a}_{Θ}	Λ^{a}_{Z}
Modelled	0.89 ± 0.02	0.98 ± 0.01	0.98 ± 0.01	0.98 ± 0.01	1.09 ± 0.01	0.98 ± 0.01
Lower thoracic aorta						
	Intima		Media		Adventitia	
	$\widehat{\lambda}^{i}_{\mathscr{X}}$	$\widehat{\lambda}^{i}_{\mathscr{Z}}$	$\widehat{\lambda}^{m}_{\mathscr{X}}$	$\widehat{\lambda}^{m}_{\mathscr{Z}}$	$\widehat{\lambda}^{a}_{\mathscr{X}}$	$\widehat{\lambda}^{a}_{\mathscr{Z}}$
Experimental	1.02 ± 0.01	0.99 ± 0.02	1.00 ± 0.01	0.97 ± 0.01	0.93 ± 0.01	1.03 ± 0.03
Modelled	1.03 ± 0.03	1.01 ± 0.03	1.02 ± 0.01	0.97 ± 0.03	0.91 ± 0.03	1.05 ± 0.05
	Λ^{i}_{Θ}	Λ^{i}_{Z}	Λ^{m}_{Θ}	Λ^{m}_{Z}	Λ^{a}_{Θ}	Λ^{a}_{Z}
Modelled	0.90 ± 0.02	1.02 ± 0.01	0.98 ± 0.01	1.02 ± 0.01	1.08 ± 0.01	1.02 ± 0.01

$\widehat{\lambda}^{k}_{i}$ denotes the components of the layer-specific deformation gradient $\mathbf{G}^{k}$ mapping an infinitesimal line element in κ_{isolated} to $\kappa_{\text{composite}}$. Λ^{k}_{i} indicates the components of the deformation gradient $\mathbf{F}_1$ mapping the deformation from $\kappa_{\text{composite}}$ to $\kappa_{\text{tension-inflation}}$. Note, the $\mathscr{x}$-direction and $\mathscr{z}$-direction in the flattened sample correspond with the circumferential and axial directions in the intact vessel, respectively. Data are presented as mean ± standard deviation.

allows the combination of intact wall and layer-specific uniaxial tensile data into a tri-layered model of a cylindrical vessel subjected to physiological loading conditions (Giudici et al., 2021a). The wall is assumed be composed of three adequately spaced membranes representing the intima, media and adventitia layers. Its composition from isolated layers to a pressurised and axially stretched cylindrical vessel requires the definition of a deformation gradient $\mathbf{G}^{k}$ for each layer k, where $k \in \{\text{i, m, a}\}$ for intima, media and adventitia. $\mathbf{G}^{k}$ maps the deformation of the isolated layer, κ_{isolated} in cartesian coordinates ($\mathscr{X}$, $\mathscr{Y}$, $\mathscr{Z}$), into a flat tri-layered wall, $\kappa_{\text{composite}}$ in cartesian coordinates ($\mathscr{x}$,$\mathscr{y}$, $\mathscr{z}$).

$$\mathbf{G}^{k} = \text{diag}\left[\frac{l_{\mathscr{x}}}{L^{k}_{\mathscr{X}}}, \quad \frac{L^{k}_{\mathscr{Y}} L^{k}_{\mathscr{Z}}}{l_{\mathscr{x}} l_{\mathscr{z}}}, \quad \frac{l_{\mathscr{z}}}{L^{k}_{\mathscr{Z}}}\right] = \text{diag}\left[\widehat{\lambda}^{k}_{\mathscr{x}}, \quad \frac{1}{\widehat{\lambda}^{k}_{\mathscr{x}}\widehat{\lambda}^{k}_{\mathscr{z}}}, \quad \widehat{\lambda}^{k}_{\mathscr{z}}\right], \tag{1}$$

where $L^{k}_{\mathscr{X}}$ and $L^{k}_{\mathscr{Z}}$ are the circumferential and axial length of the isolated layer k, $l_{\mathscr{x}}$ and $l_{\mathscr{z}}$ corresponding lengths of the tri-layered flat wall, and $\widehat{\lambda}^{k}_{\mathscr{x}}$ and $\widehat{\lambda}^{k}_{\mathscr{z}}$ define the layer-specific circumferential and axial stretches in the composite wall.

Then, $\mathbf{F}_1$ describes the deformation of the flat tri-layered wall into an unloaded cylindrical vessel, κ_{unloaded} in cylindrical coordinates (Θ, R, Z).

$$\mathbf{F}_1 = \text{diag}\left[\Lambda_{\Theta}, \quad \frac{1}{\Lambda_{\Theta}\Lambda_{Z}}, \quad \Lambda_{Z}\right]. \tag{2}$$

The axial component of $\mathbf{F}_1$, Λ_Z, is assumed to be independent from the radial coordinate, so that the incompressibility assumption leads to the following relationship for the circumferential component:

$$\Lambda_{\Theta} = \sqrt{\frac{4\pi^2 R^2_{\text{internal}}}{l^2_{\mathscr{x}}} + \frac{4\pi_{\mathscr{y}}}{l_{\mathscr{x}}\Lambda_{Z}}}, \tag{3}$$

where R_{internal} is the unloaded luminal radius.

Finally, $\mathbf{F}_2$ maps the deformation from κ_{unloaded} to the pressurised and axially stretched vessel, $\kappa_{\text{tension-inflation}}$ in cylindrical coordinates (θ, r, z).

$$\mathbf{F}_2 = \text{diag}\left[\lambda_{\theta}, \quad \frac{1}{\lambda_{\theta}\lambda_{z}}, \quad \lambda_{z}\right], \tag{4}$$

As for $\mathbf{F}_1$, the axial component of $\mathbf{F}_2$ (λ_z) is assumed to be constant throughout the wall thickness, and the circumferential deformation is inferred from conservation of volume:

$$\lambda_{\theta} = \sqrt{\left(\frac{r_{\text{internal}}}{R}\right)^2 + \frac{R^2 - R^2_{\text{internal}}}{R^2\,\lambda_{z}}}, \tag{5}$$

where r_{internal} is the luminal radius in the deformed configuration. The total deformation from isolated layer to $\kappa_{\text{tension-inflation}}$ is given by

$$\mathbf{F}_{\text{total},k} = \mathbf{F}_2\mathbf{F}_1\mathbf{G}^{k} = \text{diag}\left[\lambda_{\theta}\Lambda_{\Theta}\widehat{\lambda}^{k}_{\mathscr{x}}, \quad \frac{1}{\lambda_{\theta}\Lambda_{\Theta}\widehat{\lambda}^{k}_{\mathscr{x}}\lambda_{z}\Lambda_{Z}\widehat{\lambda}^{k}_{\mathscr{z}}}, \quad \lambda_{z}\Lambda_{Z}\widehat{\lambda}^{k}_{\mathscr{z}}\right]. \tag{6}$$

2.2.2. Layer-specific constitutive modelling

The mechanical behaviour of the isolated layers was modelled using a Holzapfel-Gasser-Ogden two fibre family strain energy function (Holzapfel-Gasser-Ogden strain energy function) (Gasser et al., 2006), that accounts for the summed contributions of an isotropic matrix and two symmetrically oriented families of collagen fibres with dispersion:

$$\Psi = \mu^{k}(I_1 - 3) + \sum_{i=1}^{2} \frac{c^{k}_{1}}{2c^{k}_{2}}\left(e^{c^{k}_{2}\left[\rho^{k} I_1 + \left(1-3\rho^{k}\right) I_{4,i} - 1\right]^2} - 1\right); \tag{7}$$

where μ^{k} is the matrix stiffness-like parameter, c^{k}_{1} is the fibre stiffness-like parameter, c^{k}_{2} is the fibre nonlinearity parameter, and $\rho \in \left[0, \frac{1}{3}\right]$ quantifies the fibre angular dispersion. I_1 and $I_{4,i}$ are the first and fourth invariants of the right Cauchy-Green deformation tensor $\mathbf{C} = \mathbf{F}^{\text{T}}\mathbf{F}$, with $i = \{1, 2\}$ indicating the two families of fibres with orientation $\alpha_{1,2} = \{\alpha, -\alpha\}$. Note that, given the phenomenological nature of the Holzapfel-Gasser-Ogden strain energy function, the fibre angle α is not meant to indicate the exact orientation of fibres in the arterial wall, but rather contribute together with ρ towards a quantification of the tissue anisotropy.

Given Eq. (7), the modelled layer stress can be calculated as

$$\mathbf{t}^{k} = -p\mathbf{I} + 2\mathbf{F}\frac{\partial \Psi}{\partial \mathbf{C}}\mathbf{F}^{\text{T}}, \tag{8}$$

where $\mathbf{I}$ is the spatial second order identity tensor, p is a Lagrange multiplier enforcing incompressibility and $\mathbf{F}$ defines a generic deformation gradient acting on the layer (Carew et al., 1968; Chuong and Fung, 1984).

2.3. Parameter estimation

The five layer-specific constitutive parameters in Eq. (7) were fitted

to the layer-specific mechanical data, minimising the error between the modelled and experimental Cauchy stresses in the circumferential and axial direction simultaneously as described before (Giudici et al., 2021a). The experimental Cauchy stress was calculated from the force-displacement mechanical data as

$$t_{ii,\mathrm{exp}} = \frac{F}{w_0 h_0}\frac{\mathscr{L}}{\mathscr{L}_0} \tag{9}$$

where F is the applied force, w_0 and h_0 are the undeformed sample width and thickness, respectively, and $\mathscr{L}$ and $\mathscr{L}_0$ are the loaded and unloaded sample inter-jaw distances, respectively.

The circumferential and axial components of the layer-specific $\mathbf{G}^k$ were estimated so that the behaviour of the tri-layered composite wall ($\kappa_{\mathrm{composite}}$) would match the experimentally determined response of the intact wall to uniaxial tensile test in both circumferential and axial directions simultaneously (Giudici et al., 2021a). The wall average Cauchy stress was calculated as

$$t_{ii}^{\mathrm{wall}} = \frac{h^{\mathrm{i}}\mathbf{t}_{ii}^{\mathrm{i}} + h^{\mathrm{m}}t_{ii}^{\mathrm{m}} + h^{\mathrm{a}}t_{ii}^{\mathrm{a}}}{h^{\mathrm{wall}}}, \tag{10}$$

where h^k is the deformed thickness of the layer k determined enforcing incompressibility, with $k = \{\mathrm{i,m,a}\}$, and $h^{\mathrm{wall}} = h^{\mathrm{i}} + h^{\mathrm{m}} + h^{\mathrm{a}}$. The layer-specific Cauchy stress in direction $i = \{x, y\}$ (t_{ii}^k) can be calculated using Eq. (8). The fitting of the layer-specific $\widehat{\lambda}_i^k$ was constrained to mean ± 3 standard deviations of values determined experimentally on the set of n=8 pig aortas used for the OA experiments. Once the best-fit $\widehat{\lambda}_i^k$ had been determined, the response of the tri-layered wall to circumferential and axial uniaxial test was analysed. The contribution provided by each layer to the total wall stress at any given stress/stretch level was calculated as

$$\text{Load bearing } \% = \frac{t_{\theta\theta}^k h^k}{t_{\theta\theta}^{\mathrm{wall}} h^{\mathrm{wall}}} \bullet 100\% \tag{11}$$

The unloaded cylindrical vessel is expected to be subjected to zero average stress in all three principal directions. Therefore, the geometrical features of $\kappa_{\mathrm{unloaded}}$ were determined so that $t_{\Theta\Theta}^{\mathrm{wall}} = 0$, $t_{RR}^{\mathrm{wall}} = 0$, and $t_{ZZ}^{\mathrm{wall}} = 0$. Note that layer-specific stresses in $\kappa_{\mathrm{unloaded}}$ are, generally, non-zero.

Since aortas were not harvested directly from euthanised animals, the *in vivo* axial length of the tested aortas was unknown. Therefore, the simulation of the physiological tension-inflation required, first, the estimation of the *in vivo* λ_z. Experimental studies have shown that the latter is close to that value of axial stretch that guarantees an approximately constant reduced axial force, $F_z = \pi\, t_{zz}^{\mathrm{wall}}\,(r_{\mathrm{external}}^2 - r_{\mathrm{internal}}^2) - \pi r_{\mathrm{internal}}^2 P$, in the physiological range of pressures (Van Loon et al., 1977). However, in a recent study, Ferruzzi et al. (2018) found that this method performs sub-optimally at the AA which is subjected to a more complex cyclic biaxial deformation. In their study, this method led to a ~36% overestimation of the true λ_z. For this reason and to investigate inter-regional differences in the response to axial deformations, here, λ_z was, first, estimated as the average cross-over point between F_z- axial stretch relationships at P = 60, 100, and 140 mmHg (λ_z^0). Then, for each artery, pressurisation in the range 0–200 mmHg was simulated while imposing three levels of axial stretch: λ_z^0, $\lambda_z^{-36\%}$ and $\lambda_z^{+36\%}$, where $\lambda_z^{-36\%} = (1-0.36)\lambda_z^0$ and $\lambda_z^{+36\%} = (1+0.36)\lambda_z^0$ correspond a 36% reduction and increase of the axial stretch, respectively. The artery pressurisation was simulated by imposing a luminal deformation and calculating the pressure *via* the Laplace equation

$$P = t_{\theta\theta}\frac{h^{\mathrm{wall}}}{r_{\mathrm{internal}}}. \tag{12}$$

Biomechanical metrics were estimated at reference pressure levels of P_{ref} = 100 and 160 mmHg, corresponding to the mean physiological resting pressure under normotensive conditions and to the a representative systolic pressure in hypertensive conditions, respectively. The intact wall and layer-specific stresses were determined using Eq. (10) and Eq. (8), respectively. The contribution provided by each layer to the total wall stress was calculated using Eq. (11).

Two metrics of circumferential material stiffness were computed: the tangential elastic modulus

$$\mathscr{K}_{\theta\theta\theta\theta} = \left.\frac{\partial t_{\theta\theta}}{\partial \varepsilon_{\theta\theta}}\right|_{P=P_{\mathrm{ref}}}, \tag{13}$$

where $\varepsilon_{\theta\theta} = \lambda_\theta - 1$, and the small-on-large stiffness (Baek et al., 2007)

$$\mathscr{C}_{\theta\theta\theta\theta} = 2(t_{\theta\theta} + p) + 4\lambda_\theta^4 \frac{\partial^2 \Psi}{\partial\left(\lambda_\theta^2\right)^2}. \tag{14}$$

From these, the corresponding structural stiffnesses were calculated as the product between the layer/wall stiffness and its loaded thickness. The elastic energy stored by the aortic wall in a cardiac cycle was estimated as

$$\Delta\Psi^{\mathrm{wall}} = \Psi^{\mathrm{wall}}\big|_{P=\mathrm{SBP}} - \Psi^{\mathrm{wall}}\big|_{P=\mathrm{DBP}}, \tag{15}$$

where Ψ^{wall} was calculated using Eq. (7) as

$$\Psi^{\mathrm{wall}} = \frac{h^{\mathrm{i}}\Psi^{\mathrm{i}} + h^{\mathrm{m}}\Psi^{\mathrm{m}} + h^{\mathrm{a}}\Psi^{\mathrm{a}}}{h^{\mathrm{wall}}}, \tag{16}$$

and systolic and diastolic blood pressure (SBP and DBP, respectively) were set to 120/80 and 160/100 mmHg for the normotensive and hypertensive scenarios, respectively.

2.4. Statistical analysis

On each aorta and at both locations, uniaxial tensile tests were run in duplicate on two circumferential and two axial strips. Constitutive modelling was then performed on two circumferential-axial pairs of samples as described previously (Giudici et al., 2021a). All presented biomechanical variables of each artery are the average of the two analyses.

Results are presented as mean ± standard deviation of the n=9 tested AAs and LTAs. Inter-layer comparisons were then performed using, first, a repeated measures ANOVA, followed by the pairwise comparisons between layers using paired student's t-tests. For each biomechanical variable of the intact wall and isolated layers, inter-regional differences were tested using student's t-tests. $p < 0.05$ was taken as statistically significant.

3. Results

3.1. Geometrical features and residual deformations

As expected, the AA was larger in diameter (mid-wall radius: 10.28±1.08 vs 7.86±0.48 mm, p<0.001) and thicker (2.55±0.24 vs 1.64±0.23 mm, p<0.001) than the LTA. Regional changes in wall thickness were mostly attributable to the decrease of the medial thickness from 1.66±0.29 to 0.84±0.21 mm (p<0.001), corresponding to 64±4% and 49±6% of the wall thickness, respectively. Intimal thickness also decreased slightly from 0.29±0.02 to 0.26±0.04 mm (p=0.021), but not adventitial thickness, which remained unchanged (0.62±0.04 vs 0.60±0.07 mm). However, its relative thicknesses, as well as that of the intima, increased from 25±3% and 12±2%, respectively, at the AA to 36±5% and 15±2% (p<0.001 for both).

When cut radially, the AA wall lost, almost entirely, its arc shape, exhibiting an OA of 140.7±22.1°. Distal LTA samples were characterised by lower residual stresses, presenting a significantly lower OA of

51.6±13.9° (p<0.001).

3.2. Layer-specific response to uniaxial testing

Individual layer stress-stretch relationships of the AA and LTA are shown in Figs. 1 and 2, respectively. Layer and region-specific strain energy function parameters are reported in Tables 2 and 3. While all tissues exhibited a pronounced nonlinear behaviour, nonlinearity was particularly evident for the adventitia. Indeed, the adventitial fibre nonlinearity parameter c_2^a was, on average, >2 and ~4 times higher than those of intima and media at the AA (intima-adventitia p=0.034 and media-adventitia p=0.007) and LTA (p<0.001), respectively.

The degree of anisotropy was layer- and region-dependent. The intimal response changed from nearly isotropic at the AA (α = 46.9± 6.7°) to markedly anisotropic at the LTA (α = 35.0± 6.7°) (p=0.002). The adventitia followed an opposite trend, moving from α = 28.9± 6.2° at the AA to 42.6±3.5° at the LTA (p<0.001), while the media showed marked anisotropy independently of the aortic location (α = 35.2± 4.7° and 32.0±4.2°, respectively). Regional differences in μ were non-significant for all layers, but the adventitia had the lowest μ at both AA (p<0.001) and LTA (p<0.01). Conversely, the fibre stiffness-like and nonlinearity parameters c_1 and c_2 were higher at the LTA than at the AA for all layers but c_1 of the adventitia, signifying distal stiffening.

3.3. Intact wall response to uniaxial testing

Intact wall stress-stretch relationships of the AA and LTA are shown in Figs. 1 and 2, respectively. The proposed tri-layered model successfully captured the complex nonlinear anisotropic behaviour of both AA (R^2 = 0.98±0.01) and LTA (R^2 = 0.98±0.02) (Fig. 3). The layer-specific circumferential and axial components of $\mathbf{G}^k$, mapping the deformation from $\kappa_{isolated}$ to $\kappa_{composite}$, are reported in Table 1. The AA showed clear anisotropy, being stiffer in the circumferential than axial direction throughout the investigated stress range. Tri-layered modelling indicated that, independently of the considered stress level and of the loading direction, the AA behaviour was largely determined by the media, bearing, on average, more than 70% of the load in both loading directions (Fig. 3A and B). Indeed, once accounted for the medial 1.03 tensile prestretch in both circumferential and axial directions, the average curves of the media in Fig. 1 closely resemble those of the intact wall.

On the other hand, the LTA intact wall exhibited a more complex response; for stress levels below ~0.10 MPa, the LTA wall was stiffer circumferentially than axially. However, its average behaviour became increasingly isotropic at higher stresses, with some aortas being even stiffer axially than circumferentially (Fig. 2). Indeed, tri-layered modelling highlighted notably different contributions from media and adventitia in circumferential and axial tests. As for the AA, the LTA wall response to circumferential uniaxial loads was dominated by the media, bearing, on average, 74–76% of the load throughout the investigated range. Furthermore, the second highest contribution was provided by the intima (17–22%), while the adventitia bore only 1–7% of the load due to the highly compressive value of $\hat{\lambda}_z^a$ (0.92±0.03) (Table 1). Conversely, the axial response of the pig LTA was dominated by the adventitia, bearing more than half of the load for stresses above 0.06 MPa. This fact was determined by two factors: first, the estimated orientation of fibres in the intima and media leaned towards the circumferential direction (α^i and α^m of the mean intimal and medial Cauchy stress-stretch relationships were 36.6° and 29.5°, respectively, Table 3) thus offering little contribution in response to axial loads. Second, our tri-layered modelling approach estimated that the adventitia was subjected to a 1.05±0.04 tensile axial prestretch in $\kappa_{composite}$, close to the 1.03±0.03 measured experimentally (Table 1), suggesting an enhanced response of adventitial collagen fibres to axial deformations applied to the composite tri-layered wall.

3.4. Simulated tension-inflation at λ_z^0

Fig. 4 shows average simulated pressure-diameter relationships of the pig AAs and LTAs at λ_z^0. Both relationships showed the typical sigmoidal shape of hyperelastic materials, however this was more accentuated at the AA. The estimated *in vivo* λ_z^0 of the AA, 1.25±0.05, was significantly higher than that of the LTA (1.07±0.04, p<0.001), as was the circumferential luminal stretch at 160 mmHg (1.40±0.06 vs 1.30±0.04, respectively, p<0.001) but not that at 100 mmHg (1.25±0.05 vs 1.23±0.03, p=0.30).

Figs. 5 and 6 present biomechanical metrics of the tension-inflation simulations at λ_z^0 of the AA and LTA, respectively. At 100 mmHg, average circumferential and axial stresses were 0.088±0.016 and 0.083±0.014 MPa at the AA, higher than those at the LTA: 0.073±0.008 (p=0.022) and 0.045±0.010 MPa (p<0.001). At both locations, the highest circumferential stress was experienced, on average, by the media, although inter-layer differences were significant only at the LTA

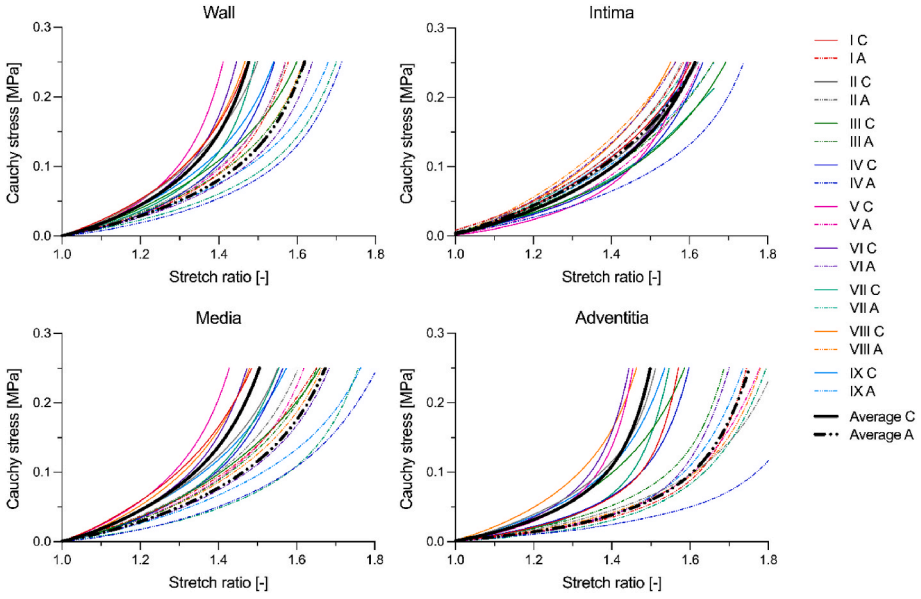

Fig. 1. Intact wall and isolated layers circumferential (C) and axial (A) experimental stress-stretch relationships of the ascending aorta of the n=9 pigs used in this study. Each relationship represents the average of two adjacent strips of the same aorta; average curves were determined as the average relationships of all n=9 pigs. For a given stretch ratio, averaging was performed in the stress direction. The difference between C and A curves progressively increases from intima to media to adventitia.

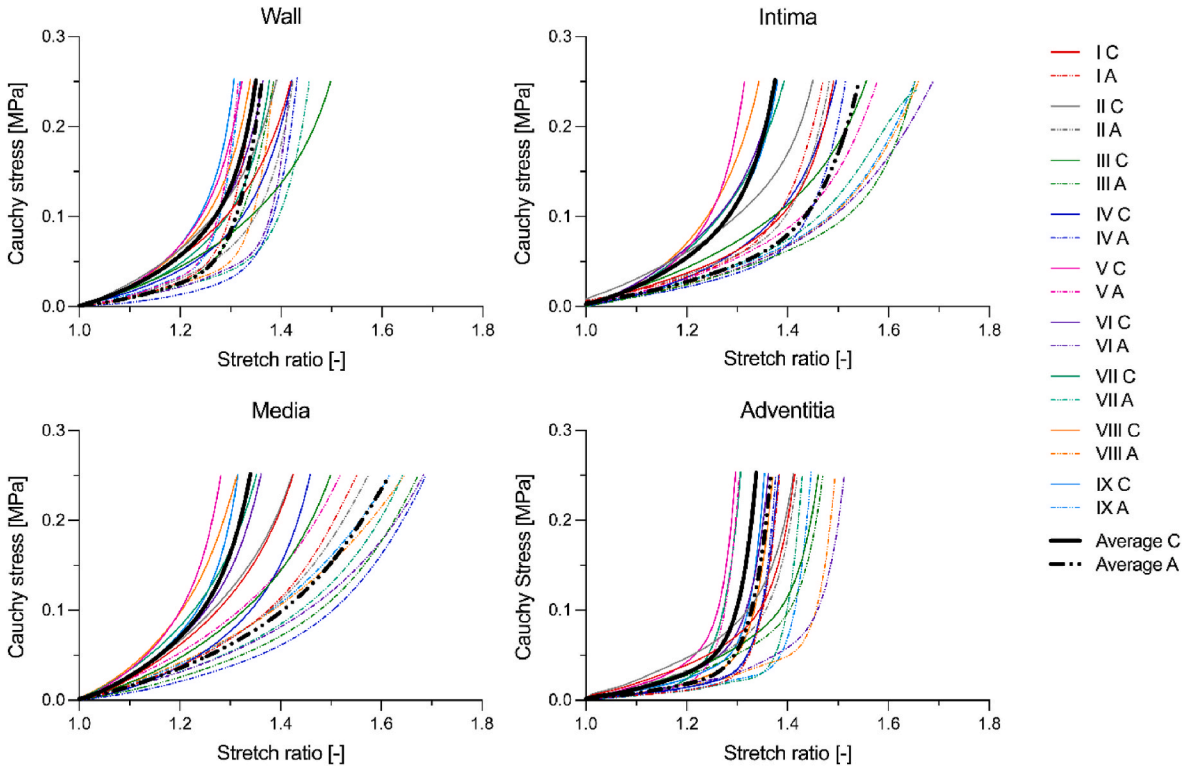

Fig. 2. Intact wall and isolated layers circumferential (C) and axial (A) experimental stress-stretch relationships of the lower thoracic aorta of the n=9 pigs used in this study. Each relationship represents the average between those of two adjacent strips taken from the same aorta. The average curves were determined as the average between relationships of all n=9 pigs. Averaging was performed between stresses at any given stretch ratio.

(Figs. 5A and 6A). As a result, at both locations, the media bore most of the circumferential load (71±8% at the AA and 57± 7% at the LTA), almost 3 times and 2 times as much as the adventitia at the AA (25± 8%) and LTA (34±8%), respectively (Fig. 7). The intimal contribution was marginal throughout the thoracic aorta (4±3% and 9± 3%, respectively). As expected, the LTA was significantly stiffer than the AA (p<0.001); the AA wall $\mathscr{K}_{\theta\theta\theta\theta}$ and $\mathscr{C}_{\theta\theta\theta\theta}$ at 100 mmHg were respectively smaller than those at LTA (0.52±0.08 and 0.62±0.10 vs 0.79± 0.16 and 0.93±0.17 MPa). Layer-specific $\mathscr{K}_{\theta\theta\theta\theta}$ and $\mathscr{C}_{\theta\theta\theta\theta}$ did not differ significantly between media and adventitia at AA, while the LTA adventitia was almost two-fold stiffer than the corresponding media layer (p<0.05 for both metrics). The stored elastic energy in the 120/80 mmHg pressure interval substantially decreased while moving distally along the aorta; medial and adventitial ΔΨ dropped by 54% and 63% (p<0.001 for both), while changes where not significant for the intima. At both locations, the media presented the highest ΔΨ (p<0.01), accounting for 71±7% and 59±7% of the total stored energy at the AA and LTA, respectively.

The wall response to the 60 mmHg pressure increase from 100 to 160 mmHg differed between AA and LTA. At the AA, the medial circumferential stress remained, on average, slightly higher, although not significantly, than that of the adventitia. As a result, the AA load partition among layers was only mildly affected, with the medial and adventitial load bearing dropping and rising by only 2± 1%, respectively. Therefore, the 113% increase in wall $\mathscr{C}_{\theta\theta\theta\theta}$ reflected relatively comparable stiffening of media (99%) and adventitia (164%). Furthermore, shifting to the 160/100 mmHg hypertensive pressure range produced comparable changes of ΔΨ in the three layers, so that only a <2% shift in stored energy was observed from the media to the adventitia. Conversely, at the LTA, increasing pressure to 160 mmHg led to a nearly equal partition of circumferential loads between media (49± 8%) and adventitia (43±9%) (Fig. 7). The 120% increase in $\mathscr{C}_{\theta\theta\theta\theta}$ was mostly driven by a three-fold increase of the adventitial stiffness, while medial and intimal $\mathscr{C}_{\theta\theta\theta\theta}$ increased by ~40–50% only. Interestingly, however, observed changes in circumferential load partition were not reflected by stored elastic energy, with the media still accounting for 56% of the total stored energy in the hypertensive range.

3.5. Simulated tension-inflation: effect of the axial stretch

$\lambda_z^{-36\%}$ and $\lambda_z^{+36\%}$ were 1.16±0.03 and 1.34±0.06 at the AA and 1.04±0.03 and 1.09±0.06 at the LTA, respectively. Supplementary Figs. S1 and S2 present the comparison between biomechanical metrics at the two levels of axial stretch for the AA and LTA, respectively. Note that these were calculated at the same level of luminal pressure: 100 mmHg for all metrics but the elastic energy that was calculated over the pressure interval 120/80 mmHg. As expected, the increase in axial stretch was associated with an 87±8% and 38±20% increase in the axial stress at the AA and LTA, respectively. However, while at the AA this change was maximal at the intima (~156%) and comparable at the media and adventitia (~80%), at the LTA, the axial stress increased relatively uniformly in the three layers: adventitia (45%), intima (43%) and media (31%). Interestingly, at both locations, the wall circumferential stress was unaffected by changes in λ_z. However, if at the AA layer-specific differences were significant only at the intima (26±34%, p<0.001), at the LTA, an 18±20% increase in adventitial circumferential stress (p=0.004) was accompanied by a 7±4% drop of that of the media (p=0.012). As a result, changes in layer-specific load bearing were negligible at the AA (intima: 4±3% → 5±3%, p = 0.001, adventitia: 25±8% → 24±8%, p=0.089, media unchanged) but not at the LTA where a ~25% increase in adventitial stiffness drove a ~5% shift in load bearing from the media (59±8% → 55±6%, p=0.003) to the outermost layer (32±9% → 37±6%, p=0.005; Fig. S3). Furthermore, at the AA, an increased axial stretch produced an increased ΔΨ across all layers and the wall normalised stored elastic energy rose by 12±2% (p<0.001). Conversely, no significant difference was observed in LTA wall's

Table 2
Layer-specific Holzapfel-Gasser-Ogden model parameters of the pig ascending aortas included in this study.

Ascending aorta							
Sample #		μ [kPa]	c_1 [kPa]	c_2 [-]	α [°]	ρ [-]	R^2
Intima	I	27.0	60.8	2.6	51.2	0.18	0.99
	II	34.7	78.6	4.7	49.7	0.28	1.00
	III	26.8	88.2	1.8	54.0	0.29	1.00
	IV	22.1	49.2	6.1	32.5	0.29	1.00
	V	16.4	144.4	1.9	44.9	0.30	0.99
	VI	28.1	127.7	0.0	50.3	0.24	1.00
	VII	25.8	95.5	0.0	54.4	0.22	1.00
	VIII	37.5	136.2	0.9	45.4	0.27	1.00
	IX	31.7	96.3	1.0	39.9	0.28	1.00
	Mean±SD	**27.8±6.0**	**97.4±31.2**	**2.1±2.0**	**46.9±6.7**	**0.26±0.04**	**1.00±0.00**
	Av. curve	**28.2**	**106.4**	**2.1**	**49.7**	**0.28**	
Media	I	27.0	145.4	1.2	35.1	0.24	1.00
	II	25.5	120.7	2.4	41.7	0.25	1.00
	III	23.0	107.8	0.9	45.0	0.27	1.00
	IV	14.9	85.2	2.2	30.5	0.25	1.00
	V	25.0	143.4	4.6	35.0	0.22	1.00
	VI	22.1	111.5	5.0	32.1	0.25	1.00
	VII	13.4	87.8	2.6	31.3	0.24	1.00
	VIII	24.7	129.3	2.6	33.9	0.24	1.00
	IX	21.0	93.2	0.8	32.1	0.24	1.00
	Mean±SD	**21.9±4.5**	**113.8±21.4**	**2.5±1.4**	**35.2±4.7**	**0.24±0.01**	**1.00±0.00**
	Av. curve	**22.8**	**124.7**	**3.3**	**30.8**	**0.27**	
Adventitia	I	12.0	44.7	9.6	26.5	0.28	1.00
	II	14.9	79.4	4.0	26.7	0.25	1.00
	III	18.3	100.0	1.8	43.9	0.26	0.99
	IV	8.1	43.7	4.5	22.6	0.25	0.99
	V	13.2	72.0	10.2	23.9	0.26	1.00
	VI	10.0	103.4	8.8	28.9	0.24	1.00
	VII	9.4	56.8	8.1	24.4	0.28	1.00
	VIII	11.3	127.6	2.2	29.6	0.23	0.99
	IX	8.9	109.7	2.8	33.8	0.23	0.99
	Mean±SD	**11.8±3.1**	**81.9±28.4**	**5.8± 3.2**	**28.9±6.2**	**0.25±0.02**	**0.99±0.00**
	Av. curve	**12.9**	**84.2**	**6.9**	**24.1**	**0.27**	

Mean±SD (standard deviation) denotes the statistical mean and standard deviation of the parameter values of all ten samples. Av. (average) curve denotes the (single) parameter value fitted to the average mechanical response (i.e., the thick black lines in Fig. 1). The average response was determined by averaging the modelled behaviour of samples I-X in both circumferential and axial directions up to a Cauchy stress of 250 kPa.

normalised stored elastic energy, although, as for the circumferential load, there was a significant 5% shift in stored energy between the media and adventitia.

4. Discussion

The mechanical properties of the arterial wall are determined by the micro and macrostructure of its three anatomical layers: the intima, the media, and the adventitia. At a microscopic level, the concentration and structural arrangements of constituents (mainly collagen, elastin and SMCs) determine their material properties. At a macroscopic level, the layers' relative thickness affects their structural stiffness and to what degree their mechanical behaviour contributes to that of wall. In the present study, using a recently introduced analytical technique that combines layer-specific uniaxial testing and tri-layered constitutive modelling (Giudici et al., 2021a), we aimed to characterise differences in the mechanical behaviour between different regions of the pig aorta, namely the ascending (AA) and the lower thoracic aorta (LTA). To the extent of our knowledge, this is the first study to apply the layer-specific testing and constitutive modelling to the healthy AA.

As expected, we found significant aortic tapering; taking the AA as a reference, the reduction in diameter at LTA was 33%, in agreement with changes reported previously (Han and Fung, 1991; Peña et al., 2015). In line with previous findings for the pig thoracic aorta (Peña et al., 2015; Sokolis, 2019), the decrease in wall thickness along the aorta followed changes in the thickness of the media, with the adventitial absolute, but not relative, thickness remaining unchanged throughout the thoracic aorta and a small decrease in intimal thickness. It is worth noting that the thicknesses found here for the isolated adventitia are higher than those measured from histological images of the wall cross-section (Sokolis, 2007). In our study, we did not perform any cross-sectional staining of the tested samples to verify the accuracy of the layer separation. While layer separation process is relatively simple, well established in the literature and the layer relative thicknesses are in line with those found in previous studies (Peña et al., 2015; Sokolis, 2019; Weisbecker et al., 2012), some suboptimal separation may have occurred. In our tri-layered modelling work, we note that the intima contributed minimally to the overall arterial wall mechanics at both locations. This finding is in agreement with well-established views on arterial mechanics (Butcher, 1960), thus, supporting our results despite possible small inaccuracies in the separation of the intima and media. However, histological images would have been helpful to judge the separation of the adventitia from the media since both layers contribute significantly to the wall mechanics. Nonetheless, the separated media and adventitia exhibited clearly different mechanical responses to loads. Especially at the LTA, our tri-layered modelling approach attributed a high-load-shielding role to the adventitia, which agrees with previous studies (Burton, 1954; Krasny et al., 2017). Hence, potential suboptimal layer separations likely did not significantly affect the validity of our findings or conclusions.

In agreement with previous studies (Peña et al., 2015; Sommer and Holzapfel, 2012; Weisbecker et al., 2013), we found considerable differences in the mechanical behaviour of the three layers, as well as differences in the response of each layer at different locations of the aorta. Consistently with previous empirical observations of highly collagenous tissues (Fonck et al., 2007; Gundiah et al., 2013), the

Table 3
Layer-specific Holzapfel-Gasser-Ogden model parameters of the pig lower thoracic aortas included in this study.

Lower thoracic aorta							
Sample #		μ [kPa]	c_1 [kPa]	c_2 [-]	α [°]	ρ [-]	R^2
Intima	I	24.05	100.5	22.2	45.8	0.25	0.97
	II	26.61	128.9	14.8	41.7	0.22	0.96
	III	16.88	98.9	2.6	38.3	0.22	0.98
	IV	14.49	101.2	13.7	41.5	0.24	0.98
	V	26.18	114.9	29.1	32.2	0.22	1.00
	VI	20.05	174.8	5.8	27.6	0.24	1.00
	VII	20.83	153.2	4.9	30.9	0.21	1.00
	VIII	19.84	197.4	9.8	26.6	0.24	1.00
	IX	20.91	125.3	11.0	30.4	0.23	1.00
	Mean±SD	**21.1±3.8**	**132.8±33.2**	**12.7±8.1**	**35.0±6.7**	**0.23±0.01**	**0.99±0.01**
	Av. curve	**19.9**	**140.2**	**16.7**	**36.6**	**0.22**	
Media	I	24.5	206.1	3.4	38.4	0.22	1.00
	II	25.7	190.9	1.9	38.2	0.20	1.00
	III	18.5	139.7	1.8	35.1	0.23	1.00
	IV	17.5	123.7	6.6	26.5	0.27	1.00
	V	44.0	146.8	33.9	32.8	0.21	1.00
	VI	27.2	135.2	9.0	27.4	0.23	1.00
	VII	25.4	184.3	4.7	31.0	0.20	1.00
	VIII	36.1	162.2	9.1	28.3	0.20	1.00
	IX	36.0	108.0	18.2	30.1	0.22	1.00
	Mean±SD	**28.3±8.3**	**155.2±31.1**	**9.8±9.7**	**32.0±4.2**	**0.22±0.02**	**1.00±0.00**
	Av. curve	**30.34**	**147.9**	**16.5**	**29.5**	**0.24**	
Adventitia	I	7.8	262.9	45.9	42.7	0.24	0.91
	II	19.8	140.0	46.3	49.5	0.25	0.98
	III	23.4	37.8	46.3	44.0	0.26	1.00
	IV	6.8	40.1	84.3	46.6	0.20	0.99
	V	12.2	202.3	82.9	42.7	0.14	0.93
	VI	14.1	35.2	60.6	37.6	0.23	1.00
	VII	5.3	54.0	96.8	40.4	0.18	0.99
	VIII	12.5	15.9	80.5	39.0	0.22	1.00
	IX	9.6	25.1	103.7	40.4	0.20	0.98
	Mean±SD	**12.4±5.7**	**90.4±84.5**	**71.9±21.3**	**42.6±3.5**	**0.21±0.03**	**0.99±0.00**
	Av. curve	**13.1**	**57.3**	**91.9**	**42.6**	**0.19**	

Mean±SD (standard deviation) denotes the statistical mean and standard deviation of the parameter values of all ten samples. Av. (average) curve denotes the (single) parameter value fitted to the average mechanical response (i.e., the thick black lines in Fig. 2). The average response was determined by averaging the modelled behaviour of samples I-X in both circumferential and axial directions up to a Cauchy stress of 250 kPa.

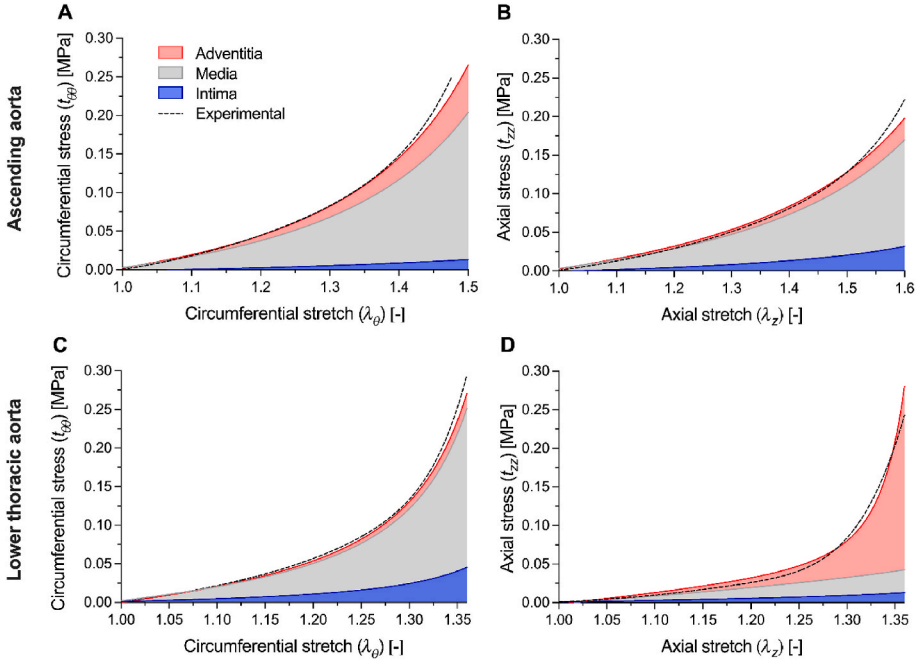

Fig. 3. Analysis of the response of the pig ascending aorta and lower thoracic aorta wall during simulated uniaxial testing using tri-layered modelling. Graphs show average stress-stretch relationship with load partitioning between layers of the n=9 pigs tested in this study. Panel A and B show the response of ascending aorta to uniaxial test in the circumferential and axial direction, respectively. Panel C and D show the response of lower thoracic aorta to uniaxial test in the circumferential and axial direction, respectively. Note that stretches on the x-axes refer to the intact wall stretch and do not account for the layer specific components of $\mathbf{G}^k$ (Table 1).

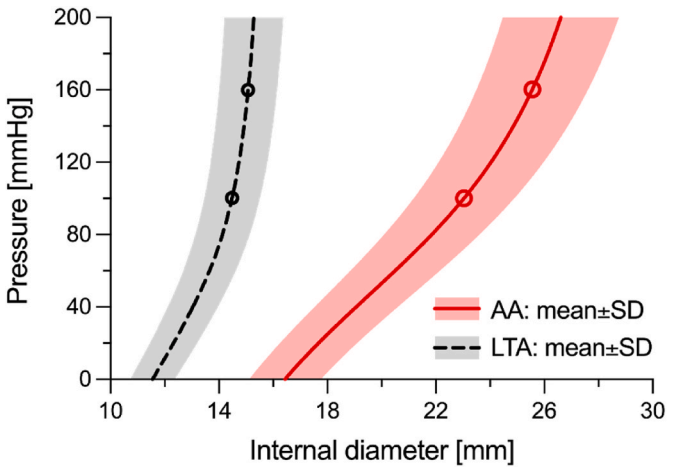

Fig. 4. Average simulated pressure diameter relationship of the n=9 pig ascending (AAs) and lower thoracic aortas (LTAs). Circles indicates the working points considered in analysis: 1) 100 mmHg, the mean physiological pressure, and 2) 160 mmHg, a representative systolic hypertensive pressure. SD, standard deviation.

adventitia was the layer exhibiting the most nonlinear behaviour, being highly compliant at low stretches and gradually stiffening at higher deformations. Interestingly, the degree of anisotropy (quantified here by the modelled collagen fibre orientation angle, Tables 2 and 3) of both intima and adventitia showed strong region-dependence; the intimal response was nearly isotropic at the AA but considerably stiffer circumferentially than axially in the distal thoracic aorta (Fig. 1). While, this shift in fibre orientation is in agreement with previous findings (Peña et al., 2015), its functional reason remains unclear. The adventitia, on the other hand, followed an opposite trend, exhibiting a highly anisotropic behaviour at the AA and a nearly isotropic behaviour in the descending thoracic aorta, both at the level of the LTA investigated in the present study and at the upper descending thoracic aorta (UTA) studied in our previous work (Giudici et al., 2021a). This finding is in disagreement with those reported by Peña et al. (2015) that found the adventitia behaved markedly anisotropically throughout the descending thoracic aorta. A possible explanation could be the different age of the animals used in their experiment: 3.5 years vs. 6–12 months in our study. This was also apparent in the ~45% larger diameter found by us compared to Peña et al. (2015) (Wolinsky and Glagov, 1969). These discordant findings might therefore be related to the maturation of the aorta into adulthood. Indeed, results in humans do suggest reorientation of fibres towards the axial direction with age (Haskett et al., 2010; Jadidi et al., 2020; Weisbecker et al., 2012). In agreement with previous studies, the anisotropy of the media in our experiments was not dependent on the aortic region (Peña et al., 2015; Weisbecker et al., 2012).

In this study, tri-layered constitutive modelling was used to investigate how observed regional differences in layer-specific mechanical behaviour affect the macroscopic response of the aortic wall. The existence of layer-specific residual stresses is known (Greenwald et al., 1997; Holzapfel et al., 2007; Peña et al., 2015), and their estimation represents the crucial link between the isolated layers' mechanical behaviour and that of the tri-layered wall (Giudici and Spronck, 2022). The most common approach to modelling of residual deformation consists of directly quantifying shape changes that strips of individual layers undergo when isolated from the wall (Díaz et al., 2021; Holzapfel et al., 2007). These include estimation of the layer-specific OA, curvature in the axial-radial plane, and changes of their circumferential and axial lengths. On the contrary, the experimental/modelling framework proposed here adopts a more pragmatic approach where layer-specific residual deformations are estimated directly from the intact wall and layer-specific mechanical data (Giudici and Spronck, 2022). The proposed approach successfully captured the complex anisotropic response to uniaxial tensile testing of both AA and LTA (Fig. 3). In our model, the multiplicative combination $\mathbf{F}_{\text{residual}} = \mathbf{F}_1\mathbf{G}^k$ represents the pre-deformation state each layer is subjected to in the unloaded vessel (Table 1). It is worth noting that at the AA the circumferential component of $\mathbf{F}_{\text{residual}}$ followed a clear gradient across the wall thickness; strongly compressive at the intima ($\Lambda^{\text{i}}_{\Theta}\widehat{\lambda}^{\text{i}}_{\theta} = 0.85$), slightly tensile at the media ($\Lambda^{\text{m}}_{\Theta}\widehat{\lambda}^{\text{m}}_{\theta} = 1.01$) and strongly tensile at the adventitia ($\Lambda^{\text{a}}_{\Theta}\widehat{\lambda}^{\text{a}}_{\theta} = 1.10$). On the contrary, at the LTA, only the intima was subjected to a considerable residual compression ($\Lambda^{\text{i}}_{\Theta}\widehat{\lambda}^{\text{i}}_{\theta} = 0.92$), while residual deformations at the media and adventitia were negligible. This finding is consistent with the much higher OA found at the AA compared to the LTA, in agreement with previous studies (Han and Fung, 1991; Saini et al., 1995). This inter-regional difference in residual stresses likely reflects the higher circumferential deformations the AA undergoes *in vivo* (Haskett et al., 2010; Wittek et al., 2016).

As hypothesised, inter-regional differences in layer-specific mechanical properties affected the mechanical behaviour of the pig aorta that differed considerably between AA and LTA. Reflecting inter-regional differences in layer-specific stiffness-like and exponential parameters, the LTA was considerably stiffer than the LTA. This result is consistent with previous findings on the human (Haskett et al., 2010) but not pig aorta (Peña et al., 2017), although, as indicated earlier, age differences might explain the difference in results. As previously shown for the UTA (Giudici et al., 2021a), increasing pressure from the physiological to the hypertensive range generated a shift in load bearing from the media to the adventitia. However, this shift was not comparable at the two locations. At the LTA, the mechanical behaviour of the adventitia appeared finely tuned to simultaneously guarantee wall compliance at physiological pressures and preserve the wall's integrity at high pressures. Indeed, adventitial circumferential stiffness nearly tripled between 100 and 160 mmHg, making the adventitia, on average, the most load-bearing layer for pressures above ~170 mmHg. On the contrary, this behaviour was not observed at the AA where the media bore more than half of the circumferential load throughout the investigated 0–200 mmHg pressure range.

AA and LTA differed also in their response to axial stretch. Interestingly, the estimated mechanically convenient λ_z^0 was much higher at the AA than at the LTA. This finding is in disagreement with experimental quantification of the axial stretch along the pig aorta (Han and Fung, 1995), suggesting that, as reported by Ferruzzi et al. (2018), the constant reduced axial force method (Van Loon et al., 1977) is suboptimal for the estimation of the *in vivo* λ_z at the AA. Ferruzzi et al. (2018) hypothesised that this characteristic would allow for λ_z of the AA to increase in response to growing level of activity (from rest to exercise), thus improving the ability of the AA to store elastic energy in systole and augment blood flow in diastole. To test this hypothesis, we simulated tension-inflation experiments at different levels of axial stretch (λ_z^0, $\lambda_z^{-36\%}$, and $\lambda_z^{+36\%}$) and used our tri-layered modelling framework to underpin the microstructural mechanism behind the observed differences. Our results seem to confirm this hypothesis; increasing λ_z allowed the AA to store greater elastic energy without affecting its mechanical behaviour and circumferential load partition among layers. This functional feature was not observed at the LTA, where increasing λ_z did not affect the wall stored energy but generated a shift in load bearing from the compliant media to the much stiffer adventitia. This functional difference is likely related to the unique anisotropy of the AA adventitia, making its circumferential behaviour less affected by axial stretching compared to both LTA and UTA (Giudici et al., 2021a).

4.1. Modelling considerations

In this work, the arterial wall was modelled as composed of three

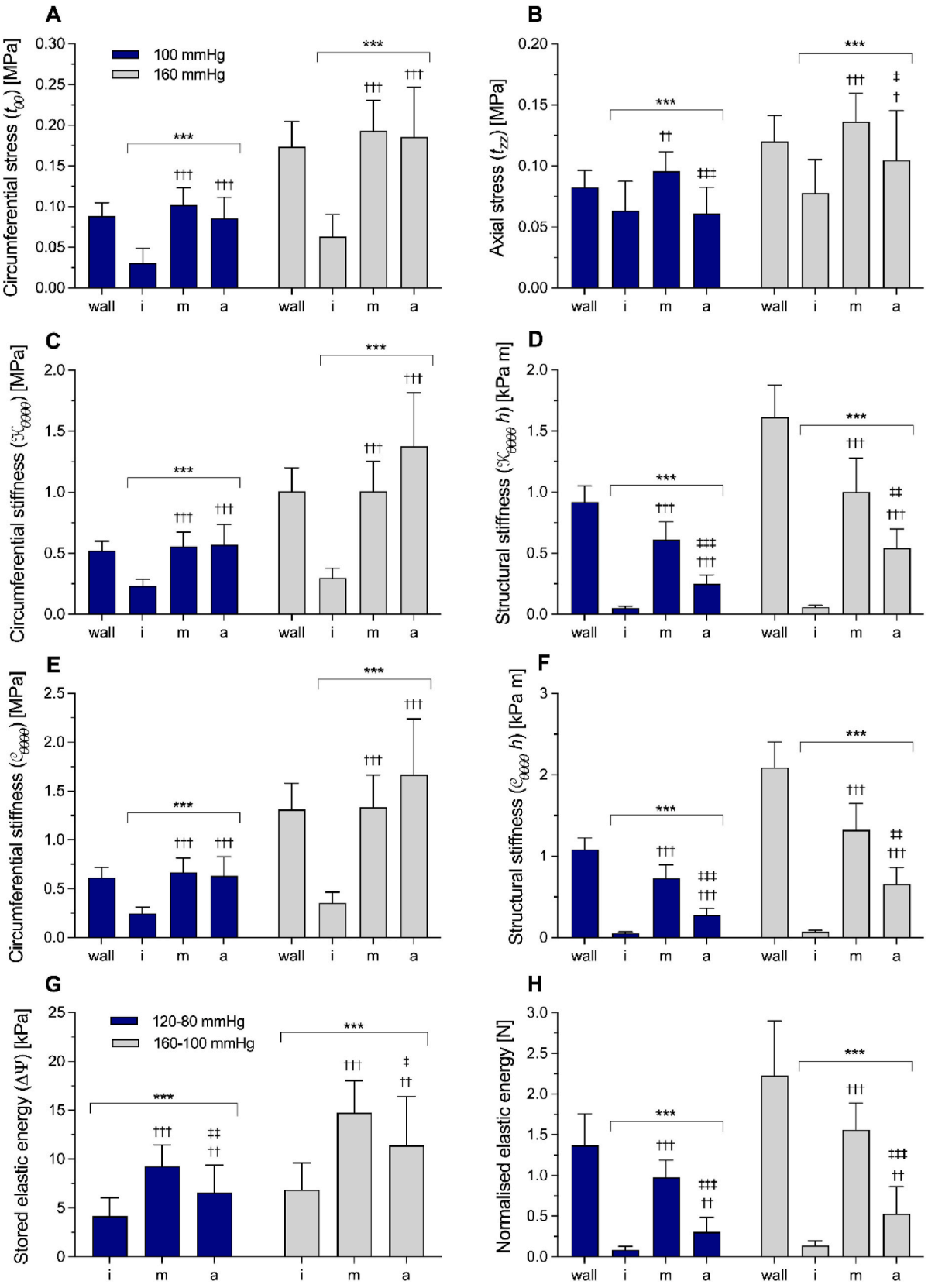

Fig. 5. Circumferential (A) and axial stress (B), circumferential stiffness (C,E), structural stiffness (D,F), stored elastic energy per unit volume (G) and stored elastic energy per unit length (H) in the pig ascending aorta at the reference pressures of 100 and 160 mmHg. wall=intact wall, i=intima, m=media, and a=adventitia. Repeated measures ANOVA: *$p < 0.05$, **$p < 0.01$ and ***$p < 0.001$. Inter-layer pairwise comparisons with paired sample student's t-tests: $^{\dagger}p < 0.05$, $^{\dagger\dagger}p < 0.01$, and $^{\dagger\dagger\dagger}p < 0.001$ vs. intima, $^{\ddagger}p < 0.05$, $^{\ddagger\ddagger}p < 0.01$, and $^{\ddagger\ddagger\ddagger}p < 0.001$ vs. media.

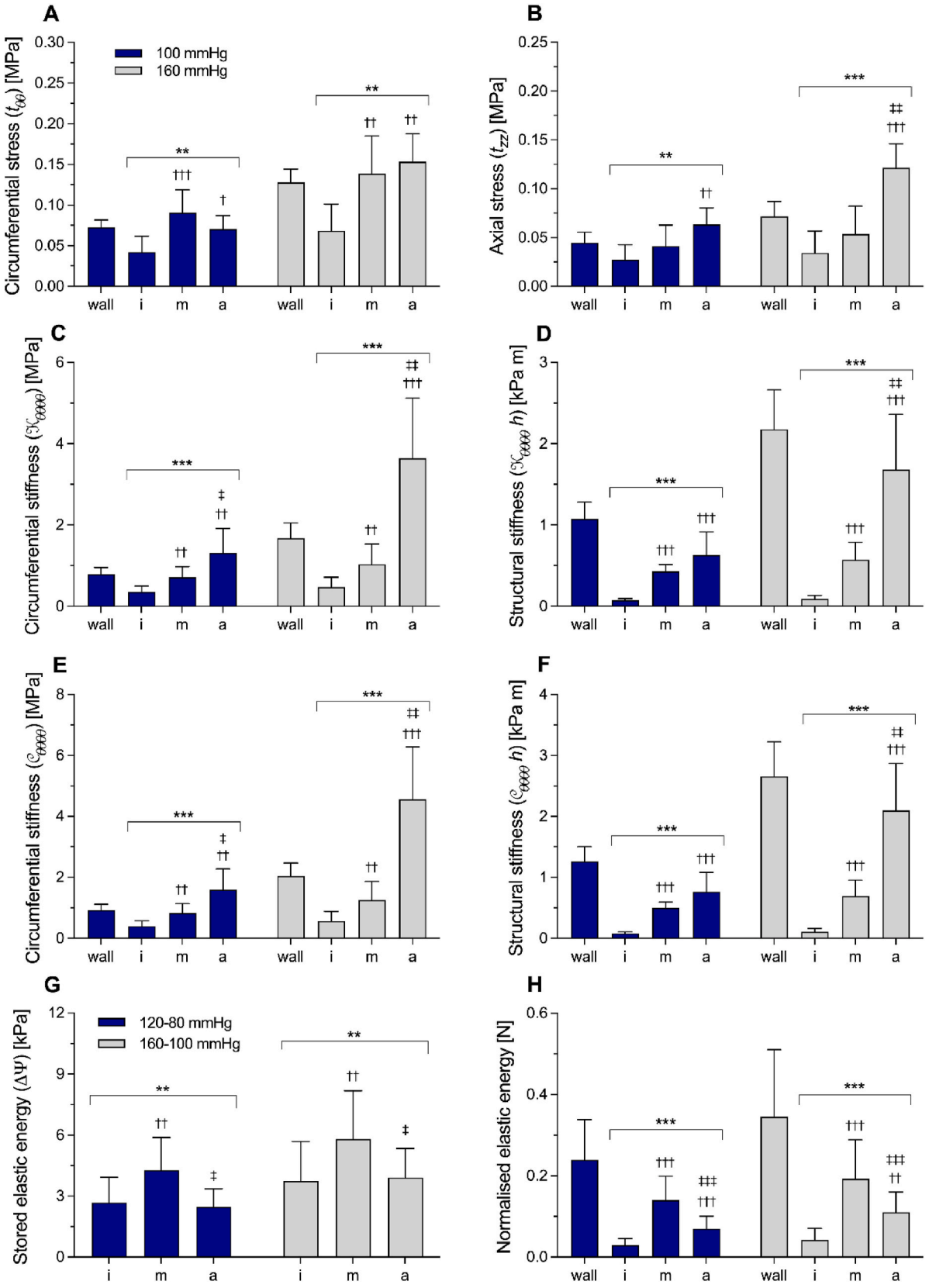

Fig. 6. Circumferential (A) and axial stress (B), circumferential stiffness (C,E), structural stiffness (D,F), stored elastic energy per unit volume (G) and stored elastic energy per unit length (H) in the pig lower thoracic aorta at the reference pressures of 100 and 160 mmHg. wall=intact wall, i=intima, m=media, and a=adventitia. Repeated measures ANOVA: $^{*}p < 0.05$, $^{**}p < 0.01$ and $^{***}p < 0.001$. Inter-layer pairwise comparisons with paired sample student's t-tests: $^{\dagger}p < 0.05$, $^{\dagger\dagger}p < 0.01$, and $^{\dagger\dagger\dagger}p < 0.001$ vs. intima, $^{\ddagger}p < 0.05$, $^{\ddagger\ddagger}p < 0.01$, and $^{\ddagger\ddagger\ddagger}p < 0.001$ vs. media.

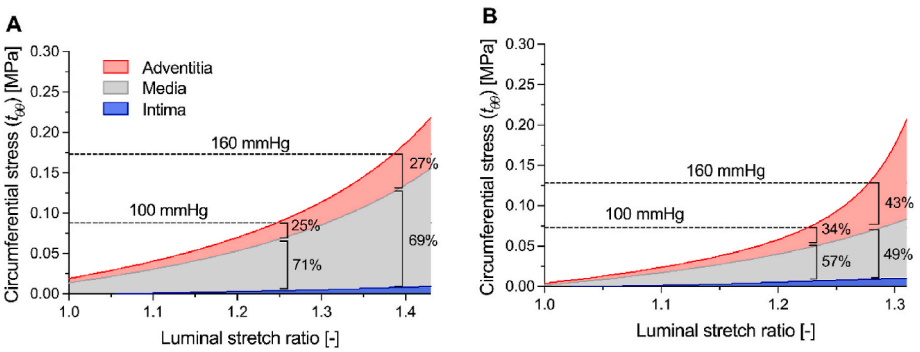

Fig. 7. Average Cauchy stress-stretch relationships with load partitioning between layers of the n=9 ascending (A) and lower thoracic aortas (B) tested in this study. Circumferential stretch at inner radius was computed as $\lambda_\theta = r_{\text{internal}}/R_{\text{internal}}$. The intimal line was obtained using Eq. (14) with $t^{\text{m}} = 0$ and $t^{\text{a}} = 0$, and the media line with $t^{\text{a}} = 0$. The adventitial line was obtained using the full version of Eq. (14).

adequately spaced membranes as previously described (Giudici et al., 2021a). This means that, in our model, each layer's loaded state is described by the average stress and deformation across the layer thickness, including residual stresses. As such, layer-specific residual stresses are also modelled as average values (Giudici and Spronck, 2022). A more detailed modelling framework which accounts for the layer-specific opening angles could improve the estimation of the distribution of stresses across the layers' thicknesses (Holzapfel and Ogden, 2010). However, the focus of this work was to study differences between two segments of the aorta in the overall mechanical response to pseudo-physiological loads and in the layer-specific relative contribution to this response, which is achievable with our thin-wall modelling approach.

4.2. Limitations

In this study, the biaxial behaviour of the isolated layers and intact wall was assessed by sequentially performing uniaxial tests in the circumferential and axial directions. Although we acknowledge that biaxial testing would have allowed to more directly assess the coupling between circumferential and axial responses to loads, earlier work has demonstrated the usefulness of sequential uniaxial testing for assessing the anisotropic mechanical properties of the arterial wall (Peña et al., 2015; Weisbecker et al., 2012). Furthermore, the deformations in the two off-axis directions were not measured throughout the uniaxial tests. Conversely, they were estimated during the layer-specific constitutive modelling fitting routine by imposing zero stress in all principal directions but that of the applied load and enforcing incompressibility. It is, therefore, possible that fitting of biaxial mechanical data could lead to different layer-specific and, consequently, different intact wall constitutive models.

The layer-specific experimental prestretches reported in Table 1 are based on the ratio between the length of intact wall and isolated layer strips before preconditioning. As described in the method, readjusting the inter-jaw distance was necessary to account for any small plastic deformation occurring in the preconditioning phase. Because preconditioning has likely affected the length of the three layers differently, the experimental prestretches reported in Table 1 may slightly differ from the actual prestretches layers were subjected to when part of the wall. This may explain the small differences found with the corresponding modelled values (Table 1).

Using a digital micrometer, we measured the arterial wall and isolated layer strips at three locations along their length to estimate their average thickness. However, we acknowledge the circumferential variation in the thickness of the aortic wall (Kim and Baek, 2011) and, hence, the difficulty associated with its measurement. Alternative methods to assess the thickness-length profile or directly measure the average thickness of the strip (e.g., by positioning the strip between two glass slides) might have improved the quantification of the wall thickness.

The simulated physiological loads consisted of the inflation of the tubular artery held at a constant axial stretch, estimating biomechanics variables at both mean physiological pressure (100 mmHg) and representative hypertensive systolic pressure (160 mmHg). While this simulation is appropriate for the descending thoracic aorta, it represents a simplification of reality for the AA, that is subjected to simultaneous cyclic pressurisation, axial stretch and twist *in vivo* (Wittek et al., 2016). Although the reported stored elastic energy over the cardiac cycle necessarily underestimates the *in vivo* value, replication of the tension-inflation simulations at different level of axial stretch showed that the AA's circumferential tri-layered mechanics is almost unaffected by axial elongation.

5. Conclusions

In the present study, we combined layer-specific mechanical testing and tri-layered constitutive modelling to provide novel insight into the biomechanical and functional differences between the pig ascending and lower thoracic aorta. While, as expected, we observed considerable distal stiffening of the aorta, our approach highlighted other important differences in the mechanical behaviour between aortic regions. First, the ascending aorta exhibits a higher degree of anisotropy (especially at high deformations) compared to the lower thoracic aorta. This difference is due to inter-regional differences in mechanical properties of the adventitia, which is nearly isotropic in the low thoracic region and relatively unresponsive to axial deformations in the ascending region. Second, residual stresses are much higher at the ascending than at lower thoracic aorta. Together, these differences in biomechanics lead to functional differences between regions. At the lower thoracic aorta, the adventitia works as a protective layer that preserves structural integrity against excessive circumferential and axial loads. Conversely, this function is not observed at ascending aorta, where the compliant media remains the most load-bearing layer over wide ranges of biaxial deformations. Hence, this unique feature may allow the ascending aorta to increase elastic energy storage in response to increased physical exertion and, consequently, maximise its diastolic function.

Funding sources

This work was supported by the ARTERY (Association for Research into Arterial Structure and Physiology) society (2019 Research Exchange Grant to A.G.) and by the European Union's Horizon 2020 Research and Innovation program (Grant 793805 to B.S.).

CRediT authorship contribution statement

A. Giudici: Writing – original draft, Software, Project administration, Methodology, Investigation, Formal analysis, Data curation, Conceptualization. **B. Spronck:** Writing – review & editing, Supervision, Methodology, Conceptualization. **I.B. Wilkinson:** Writing – review & editing, Supervision, Conceptualization. **A.W. Khir:** Writing – review & editing, Supervision, Conceptualization.

Declaration of competing interest

The authors declare that they have no known competing financial interests or personal relationships that could have appeared to influence the work reported in this paper.

Data availability

Data will be made available on request.

Acknowledgements:

We thank Jay D. Humphrey for his support and valuable advice.

Appendix A. Supplementary data

Supplementary data to this article can be found online at https://doi.org/10.1016/j.jmbbm.2023.105752.

References

Apter, J., Rabinowitz, M., Cummings, D., 1966. Correlation of visco-elastic properties of large arteries with microscopic structure. Circ. Res. 19, 104–121.
Baek, S., Gleason, R.L., Rajagopal, K.R., Humphrey, J.D., 2007. Theory of small on large: potential utility in computations of fluid-solid interactions in arteries. Comput. Methods Appl. Mech. Eng. 196, 3070–3078.
Burton, A.C., 1954. Relation of structure to function of the tissues of the wall of blood vessels. Physiol. Rev. 34, 619–642.
Butcher, H.R.J., 1960. The elastic properties of human aortic intima, media and adventitia: the initial effect of thromboendarterectomy. Ann. Surg. 151, 480–489.
Carew, T.E., Vaishnav, R.N., Patel, D.J., 1968. Compressibility of the arterial wall. Circ. Res. 23, 61.
Chuong, C.J., Fung, Y.C., 1986. On residual stresses in arteries. J. Biomech. Eng. 108, 189–192.
Chuong, C.J., Fung, Y.C., 1984. Compressibility and constitutive equation of arterial wall in radial compression experiments. J. Biomech. 17, 35–40.
Cox, R., 1978. Regional variation of series elasticity in canine arterial smooth muscles. Am. J. Physiol. 234.
Cox, R.H., 1978. Passive mechanics and connective tissue composition of canine arteries. Am. Physiol. Soc. 234, H533–H541.
Deveja, R.P., Iliopoulos, D.C., Kritharis, E.P., Angouras, D.C., Sfyris, D., Papadodima, S. A., Sokolis, D.P., 2018. Effect of aneurysm and bicuspid aortic valve on layer-specific ascending aorta mechanics. Ann. Thorac. Surg. 106, 1692–1701.
Díaz, C., Peña, J.A., Martínez, M.A., Peña, E., 2021. Unraveling the multilayer mechanical response of aorta using layer-specific residual stresses and experimental properties. J. Mech. Behav. Biomed. Mater. 113, 104070.
Dinardo, C.L., Venturini, G., Zhou, E.H., Watanabe, I.S., Campos, L.C.G., Dariolli, R., da Motta-Leal-Filho, J.M., Carvalho, V.M., Cardozo, K.H.M., Krieger, J.E., Alencar, A. M., Pereira, A.C., 2014. Variation of mechanical properties and quantitative proteomics of VSMC along the arterial tree. Am. J. Physiol. Heart Circ. Physiol. 306, 505–516.
Ferruzzi, J., Achille, P. Di, Tellides, G., Humphrey, J.D., 2018. Combining in vivo and in vitro biomechanical data reveals key roles of perivascular tethering in central artery function. PLoS One 13, 1–21.
Fischer, G., Llaurado, J., 1966. Collagen and elastin content in canine arteries selected from functionally different vascular beds. Circ. Res. 19, 394–399.
Fonck, E., Prod'hom, G., Roy, S., Augsburger, L., Rüfenacht, D.A., Stergiopulos, N., 2007. Effect of elastin degradation on carotid wall mechanics as assessed by a constituent-based biomechanical model. Am. J. Physiol. Heart Circ. Physiol. 292, 2754–2763.
Gasser, T.C., Ogden, R.W., Holzapfel, G.A., 2006. Hyperelastic modelling of arterial layers with distributed collagen fibre orientations. J. R. Soc. Interface 3, 15–35.
Giudici, A., Khir, A.W., Szafron, J.M., Spronck, B., 2021a. From uniaxial testing of isolated layers to a tri-layered arterial wall: a novel constitutive modelling framework. Ann. Biomed. Eng. 49, 2454–2467.
Giudici, A., Spronck, B., 2022. The role of layer-specific residual stresses in arterial mechanics: analysis via a novel modelling framework. Artery Res. 28, 41–54.
Giudici, A., Wilkinson, I.B., Khir, A., 2021b. Review of the techniques used for investigating the role elastin and collagen play in arterial wall mechanics. IEEE Rev. Biomed. Eng. 14, 256–269.
Greenwald, S.E., Moore, J.J.E., Rachev, A., Kane, T.P.C., Meister, J.-J., 1997. Experimental investigation of the distribution of the residual strains in the arterial wall. Trans. ASME 119, 438–444.
Gundiah, N., Babu, A.R., Pruitt, L.A., 2013. Effects of elastase and collagenase on the nonlinearity and anisotropy of porcine aorta. Physiol. Meas. 34, 1657–1673.
Han, H.C., Fung, Y.C., 1995. Longitudinal strain of canine and porcine aortas. J. Biomech. 28, 637–641.
Han, H.C., Fung, Y.C., 1991. Species dependence of the zero-stress state of aorta: pig versus rat. J. Biomech. Eng. 113, 446–451.
Harkness, M.L.R., Harkness, R.D., McDonald, D.A., 1957. The collagen and elastin content of the arterial wall in the dog. Proc. R. Soc. Lond. Ser. B Biol. Sci. 146, 541–551.
Haskett, D., Johnson, G., Zhou, A., Utzinger, U., Vande Geest, J., 2010. Microstructural and biomechanical alterations of the human aorta as a function of age and location. Biomech. Model. Mechanobiol. 9, 725–736.
Holzapfel, G., Sommer, G., Auer, M., Regitnig, P., Ogden, R., 2007. Layer-specific 3D residual deformations of human aortas with non-atherosclerotic intimal thickening. Ann. Biomed. Eng. 35, 530–545.
Holzapfel, G.A., Gasser, C.T., Sommer, G., Regitnig, P., 2005. Determination of layer-specific mechanical properties of human coronary arteries with nonatherosclerotic intimal thickening and related constitutive modeling. Am. J. Physiol. 289, H2048–H2058.
Holzapfel, G.A., Ogden, R.W., 2010. Modelling the layer-specific three-dimensional residual stresses in arteries, with an application to the human aorta. J. R. Soc. Interface 7, 787–799.
Holzapfel, G.A., Stadler, M., Schulze-Bauer, C.A.J., 2002. A layer-specific three-dimensional model for the simulation of balloon angioplasty using magnetic resonance imaging and mechanical testing. Ann. Biomed. Eng. 30, 753–767.
Jadidi, M., Habibnezhad, M., Anttila, E., Maleckis, K., Desyatova, A., MacTaggart, J., Kamenskiy, A., 2020. Mechanical and structural changes in human thoracic aortas with age. Acta Biomater. 103, 172–188.
Kim, J., Baek, S., 2011. Circumferential variations of mechanical behavior of the porcine thoracic aorta during the inflation test. J. Biomech. 44, 1941–1947.
Krasny, W., Morin, C., Magoariec, H., Avril, S., 2017. A comprehensive study of layer-specific morphological changes in the microstructure of carotid arteries under uniaxial load. Acta Biomater. 57, 342–351.
Krüger-Genge, A., Blocki, A., Franke, R.P., Jung, F., 2019. Vascular endothelial cell biology: an update. Int. J. Mol. Sci. 20, 4411.
Learoyd, B.M., Taylor, M.G., 1966. Alterations with age in the viscoelastic properties of human arterial walls. Circ. Res. 18, 278–292.
Lu, X., Zhao, J.B., Wang, G.R., Gregersen, H., Kassab, G.S., Kassab, G.S., 2001. Remodeling of the Zero-Stress State of Femoral Arteries in Response to Flow Overload.
Peña, J.A., Corral, V., Martínez, M.A., Peña, E., 2017. Over length quantification of the multiracial mechanical properties of the ascending, descending and abdominal aorta using Digital Image Correlation. J. Mech. Behav. Biomed. Mater. 77, 434–445.
Peña, J.A., Martinez, M.A., Peña, E., 2015. Layer-specific residual deformations and uniaxial and biaxial mechanical properties of thoracic porcine aorta. J. Mech. Behav. Biomed. Mater. 50, 55–69.
Rachev, A., Greenwald, S.E., 2003. Residual strains in conduit arteries. J. Biomech. 36, 661–670.
Saini, A., Berry, C., Greenwald, S., 1995. The effect of age and sex on residual stress. J. Vasc. Res. 32, 398–405.
Sassani, S.G., Tsangaris, S., Sokolis, D.P., 2015. Layer- and region-specific material characterization of ascending thoracic aortic aneurysms by microstructure-based models. J. Biomech. 48, 3757–3765.
Sokolis, D.P., 2019. Regional distribution of layer-specific circumferential residual deformations and opening angles in the porcine aorta. J. Biomech. 96, 109335.
Sokolis, D.P., 2007. Passive mechanical properties and structure of the aorta: segmental analysis. Acta Physiol. 190, 277–289.
Sommer, G., Holzapfel, G.A., 2012. 3D constitutive modeling of the biaxial mechanical response of intact and layer-dissected human carotid arteries. J. Mech. Behav. Biomed. Mater. 5, 116–128.
Sommer, G., Regitnig, P., Költringer, L., Holzapfel, G.A., 2010. Biaxial mechanical properties of intact and layer-dissected human carotid arteries at physiological and supraphysiological loadings. Am. J. Physiol. Heart Circ. Physiol. 298, 898–912.
Teng, Z., Feng, J., Zhang, Y., Huang, Y., Sutcliffe, M.P.F., Brown, A.J., Jing, Z., Gillard, J. H., Lu, Q., 2015. Layer- and direction-specific material properties, extreme extensibility and ultimate material strength of human abdominal aorta and aneurysm: a uniaxial extension study. Ann. Biomed. Eng. 43, 2745–2759.
Vaishnav, R.N., Vossoughi, J., 1983. Estimation of the residual strains in aortic segments. Proc. Second South. Biomed. Eng. Conf. 330–333.
Van Loon, P., Klip, W., Bradley, E.L., 1977. Length-force and volume-pressure relationships of arteries. Biorheology 14, 181–201.
Weisbecker, H., Pierce, D.M., Regitnig, P., Holzapfel, G.A., 2012. Layer-specific damage experiments and modeling of human thoracic and abdominal aortas with non-atherosclerotic intimal thickening. J. Mech. Behav. Biomed. Mater. 12, 93–106.
Weisbecker, H., Viertler, C., Pierce, D.M., Holzapfel, G.A., 2013. The role of elastin and collagen in the softening behavior of the human thoracic aortic media. J. Biomech. 46, 1859–1865.
Wittek, A., Karatolios, K., Fritzen, C.P., Bereiter-Hahn, J., Schieffer, B., Moosdorf, R., Vogt, S., Blase, C., 2016. Cyclic three-dimensional wall motion of the human

ascending and abdominal aorta characterized by time-resolved three-dimensional ultrasound speckle tracking. Biomech. Model. Mechanobiol. 15, 1375–1388.
Wolinsky, H., Glagov, S., 1969. Comparison of abdominal and thoracic aortic medial structure in mammals. Circ. Res. 25, 677–686.
Wolinsky, H., Glagov, S., 1964. Structural basis for the static mechanical properties of the aortic media. Circ. Res. 14, 400–413.

Glossary

κ_{isolated}: configuration of the isolated layer in cartesian coordinates ($\mathscr{X}$, $\mathscr{Y}$, $\mathscr{Z}$)
$\kappa_{\text{composite}}$: configuration of the composite tri-layered wall slab in cartesian coordinates (x, y, z)
κ_{unloaded}: configuration of the unloaded tri-layered artery in cylindrical coordinates (Θ, R, Z)
$\kappa_{\text{tension-inflation}}$: configuration of the loaded tri-layered artery in cylindrical coordinates (θ, r, z)
$\mathbf{G}^k$: deformation gradient from κ_{isolated} to $\kappa_{\text{composite}}$ for the layer k
$\widehat{\lambda}_i^k$: component of $\mathbf{G}^k$ in direction $i = \{x, y, z\}$.
$\mathbf{F}_1$: deformation gradient from $\kappa_{\text{composite}}$ to κ_{unloaded}
Λ_i: component of F_1 in direction $\mathrm{i} = \{\Theta, \mathrm{R}, \mathrm{Z}\}$.
F_2: deformation gradient from κ_{unloaded} to $\kappa_{\text{tension-inflation}}$
λ_i: component of F_2 in direction $i = \{\theta, \mathrm{r}, \mathrm{z}\}$.
R_{internal}: luminal radius in κ_{unloaded}
r_{internal}: luminal radius in $\kappa_{\text{tension-inflation}}$
h^{wall}: wall thickness in $\kappa_{\text{tension-inflation}}$
h^k: thickness of the layer k in $\kappa_{\text{tension-inflation}}$
Ψ: strain energy density function
μ^k: elastin stiffness-like parameter for the layer k
k_1^k: collagen stiffness-like parameter for the layer k
k_2^k: collagen nonlinearity parameter for the layer k
α^k: collagen fibre orientation parameter for the layer k
ρ^k: collagen fibre dispersion parameter for the layer k
$\mathbf{t}$: Cauchy stress tensor
$\mathscr{K}_{\theta\theta\theta\theta}$: circumferential tangential elastic modulus
$\mathscr{C}_{\theta\theta\theta\theta}$: small-on-large circumferential stiffness